Journal of Sound and Vibration 329 (2010) 3679–3690

Contents lists available at ScienceDirect

Journal of Sound and Vibration

journal homepage: www.elsevier.com/locate/jsvi

Acoustic forcing to simulate the plunging motion of an airfoil

W.F.J. Olsman [a,*], J.F.H. Willems [a], S.J. Hulshoff [b], A. Hirschberg [a], R.R. Trieling [a]

[a] Department of Applied Physics, Eindhoven University of Technology, PO Box 513, 5600 MB Eindhoven, The Netherlands
[b] Faculty of Aerospace Engineering, Delft University of Technology, PO Box 5058, 2600 GB Delft, The Netherlands

ARTICLE INFO

Article history:
Received 24 August 2009
Received in revised form
26 March 2010
Accepted 30 March 2010
Handling Editor: D. Juve
Available online 24 April 2010

ABSTRACT

An alternative to performing dynamic plunging measurements on an airfoil is presented, which is suitable for high reduced frequencies. Instead of physically displacing the airfoil, the flow is modulated by loudspeakers. The loudspeakers are tuned to the first transversal eigenfrequency of the wind tunnel, which results in a 2D acoustic field. The paper first describes the experimental investigation of the acoustic field without a main flow. Then results of acoustic field measurements are compared to a commercially available boundary-element method. The results of local pressure measurements on the airfoil are compared to predictions of a numerical solution of the Euler equations for in inviscid compressible flow. This solution includes the acoustic field. A strong point of the method is that the excitation amplitude can be varied easily.

1. Introduction

The work presented in this paper was carried out within the framework of the European project VortexCell2050 [1]. The goal of this project is to design a relatively thick wing without massive vortex shedding. In order to prevent downstream vortex shedding, the vortex is trapped in a cavity in the wing.

Our long term goal is to gain insight into the dynamical behavior of such a wing with a cavity. We will argue that significant effects of a cavity may be expected at reduced frequencies much higher than commonly encountered in the study of the flutter of wings. This calls for the development of an alternative experimental method. In the present paper we explore the potential of a new method to perform unsteady measurements on an airfoil, using acoustic forcing.

A lot of research has been performed on rectangular cavities in plane walls. In contrast, not much literature is available for the case of a cavity placed in an airfoil. It was shown by Rockwell and Naudasher [2] that a cavity in a plane wall can display a shear layer instability mode when the Strouhal number,[1] $k_W = \omega W/U_\infty$, is of order 3, where W is the opening of the cavity, ω is the angular frequency in rad/s and U_∞ in the main stream velocity. The cavity may also give rise to a cavity wake mode, described by Gharib and Roshko [3], however this mode is rarely observed in experiments. A Strouhal number $k_W \approx 3$ with an opening of the cavity of $W=2b/5$, with b the semi-chord of the airfoil, implies a reduced frequency $k_b = \omega b/U_\infty \approx 8$, which is for an airfoil a high value of the reduced frequency.

* Corresponding author.
E-mail address: w.f.j.olsman@tue.nl (W.F.J. Olsman).

[1] Note that in the literature concerning cavities the Strouhal number is usually defined as fW/U_∞, with W the opening of the cavity, U_∞ the free stream velocity and f the frequency in Hz. In the literature about dynamical behavior of airfoils the Strouhal number is defined as $k_b = \omega b/U_\infty$, with b the half chord of the airfoil and ω the angular frequency in rad/s, the subscript b denotes that the half chord was used as a reference length. This last definition of the Strouhal number corresponds to the definition of the reduced frequency in the literature about flutter, in this paper we will use this definition of the Strouhal number.

0022-460X/$ - see front matter © 2010 Elsevier Ltd. All rights reserved.
doi:10.1016/j.jsv.2010.03.034

The conventional method for dynamic measurements on an airfoil is to mount the airfoil on a rig, which is displaced with respect to the main flow by a mechanical system, see Halfman [4] and Schewe et al. [5]. It is a challenge to design a setup light and stiff enough to prevent its eigenfrequencies from interfering with the measurements. It is difficult to reach high values of the reduced frequency due to the inertia of the moving parts of the setup. With the proposed alternative method, in which the airfoil is fixed to the wind tunnel walls and the flow is modulated by loudspeakers, these problems are avoided and there is no need for a complex mechanical system to displace the airfoil. By exciting the system at the first acoustical transversal resonance frequency high fluctuating velocity amplitudes can be reached, with reasonably uniform excitation. With this alternative method it is possible to conduct high reduced frequency dynamical measurements on an airfoil. Acoustic excitation has been considered as a means to study the stalled flow over an airfoil at low speed by Zaman [6]. The effect of acoustic excitation of the laminar boundary layer was investigated by Archibald [7]. However, to our knowledge, acoustic excitation has not been used in order to obtain information on the dynamical response of airfoils at high Reynolds numbers. Furthermore there was no quantitative description of the acoustic field around the airfoil.

Quantitative implementation of the measurement method involves an analysis of the acoustic response of the wind tunnel to acoustic excitation. The acoustic field in an infinite duct with uniform subsonic flow was studied numerically by Mosher [8]. Prediction of acoustic resonant frequencies in wind tunnel test sections with plenum chambers, assuming infinite length in stream wise direction and uniform flow is provided by Lee [9].

In the wind tunnel considered here, the test section is connected on the upstream side to the settling chamber by a contraction and on the down stream side to the diffusor. Between the end of the test section and the inlet of the diffusor there is a slit. The purpose of this slit is to prevent a very low pressure in the test section. Since both the contraction and the slit/diffusor are area expansions, this implies that they will partially reflect acoustic waves. A duct segment with two open ends shows therefore qualitatively the same acoustic behavior as the test section placed in the wind tunnel.

The acoustic field in the test section, decoupled from the wind tunnel, is investigated in an anechoic room and experimental results are compared to results of a numerical indirect boundary element method (IBEM). Also the influence of the wing on the acoustic field inside the test section is investigated. Then the acoustic field inside the test section placed in the wind tunnel is discussed. The main aim of this study of the acoustic field is to assess the procedure for experimental determination of the transversal acoustic velocity driving the flow around the wing. This procedure is not trivial due to the shape of the acoustic field and wall vibrations. Wall vibrations can pollute the acoustic field, which may lead to the appearance of two resonance peaks. One peak related to an acoustic resonance and the other related to a resonance of the wall, which causes the entire wall acting as a loudspeaker. Furthermore wall vibrations may corrupt the signals from microphones mounted directly in the wall.

The relation between acoustically forcing the airfoil and the plunging motion of the airfoil is explained in Section 5.4 and lastly the results of measurements on a standard NACA0018 airfoil is presented and compared with the results of 2D Euler simulations and linearised potential flow theory described in Fung [10].

2. Experimental method

The test facility is a low-speed wind tunnel with a test section with square cross section 500 mm × 500 mm, and a length of 1000 mm. The walls of the test section are manufactured from plywood with a wall thickness of 24 mm. They are reinforced with wooden ribs of 100 mm height and 36 mm width, to reduce the effects of wall vibrations. Ribs meeting at junctions of walls are connected by means of L-shaped steel plates (150 mm × 150 mm × 4 mm). The maximum velocity in the test section is about 67 m/s, which corresponds to a free stream Mach number of $M_\infty = 0.19$ at room temperature. The velocity is determined by measuring the pressure difference between the settling chamber and the test section with a water manometer, neglecting the velocity in the settling chamber. The velocity is determined with an accuracy of 0.2%. The turbulence intensity in the empty test section is less than 0.2%.

In each of the two opposite side walls of the test section a circular hole with a diameter of 200 mm, covered with fabric, has been made. On the outside of the test section two speakers (JBL 2206H) are mounted over these holes, one on each side of the test section. The loudspeakers are not fixed to the test section but mounted on an independent rigid aluminium frame. The slit between the test section wall and the rim of the loudspeaker is filled with a 5 mm thick rim of closed-cell foam. This provides an acoustical seal with a minimum of mechanical contact. The speakers are connected in series and out of phase, such that both membranes have displacements in the same direction with respect to each other. The speakers are driven by an amplifier (QSC RMX2450) which in turn is driven by a function generator (Yokogawa FG120). In both side walls and the top wall of the test section piezoelectric pressure transducers (PCB 116A or Kistler 7031) are mounted. The transducers are positioned in order to measure the acoustic field. The transducers are mounted on a 1 cm thick layer of closed-cell foam, which is glued to the wall of the test section. They have been mounted such that there is no direct mechanical contact with the wall. The eigenfrequency of the microphone with foam suspension is tuned to be significantly below the frequency at which the speakers are driven. This isolates the microphones from wall vibrations. The microphones are acceleration compensated in the axial direction but display strong errors when fixed rigidly in a vibrating wall. A top view of the test section is given in Fig. 1, some of the stiffeners are also shown in this view. The origin of the coordinate system used is in the lower left inside of the test section in Fig. 1. The locations of the microphones are shown in Fig. 1, by the labels M1–M5. The type of microphone and its exact mounting location are given in Table 1.

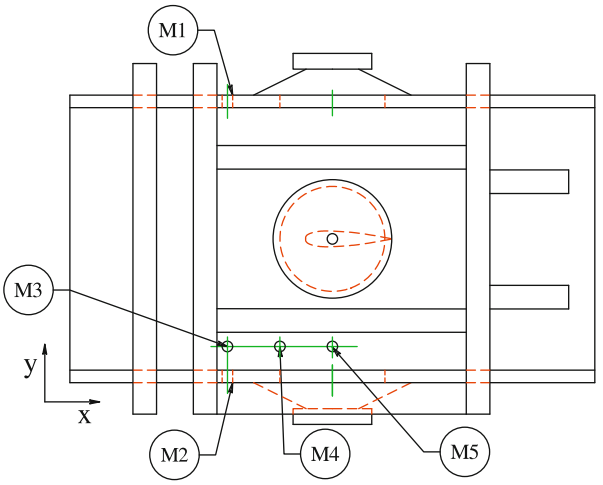

Fig. 1. Top view of the test section of the wind tunnel with speakers mounted and the airfoil placed in the middle. The pressure transducers mounted in the side and top walls are indicated with M1–M5. The flow through the test section is from left to right.

Table 1
Position and type of microphones placed in the walls of the test section.

Microphone	Position (x,y,z) (mm)	Type
M1	(300, 500.0, 250)	Kistler 7031
M2	(300, 0.0, 250)	PCB 116A
M3	(300, 45.0, 500)	Kistler 7031
M4	(400, 45.0, 500)	Kistler 7031
M5	(500, 45.0, 500)	PCB 116A

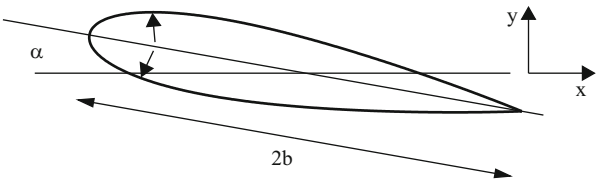

Fig. 2. NACA0018 profile with chord $2b$=165 mm. The location of the pressure transducers is indicated by the arrows inside the profile. The angle of attack is defined positive as indicated in the figure.

In the middle of the test section a NACA0018 profile is mounted vertically. The airfoil is manufactured out of extruded aluminium and approximates the NACA0018 profile definition within an accuracy of 0.2 mm. The chord $2b$ of the airfoil is 165 mm and the width is 495 mm such that it spans the entire test section from top to bottom, closing tightly at the ends. The vertical positioning of the airfoil provides practical advantages related to the placement of experimental equipment. The bottom of the airfoil is fixed by a pin-in-hole connection. The top is connected by a tube to a flange which is bolted to the test section. This allows for modification of the angle of attack, α defined in Fig. 1, of the airfoil, which can be set with an accuracy of 0.5°. At $\alpha = 0$ the blockage in the test section is 2%.

In the airfoil two miniature dynamic pressure transducers (Kulite XCS-093-140mBarD) are placed flush to the surface, on either side of the airfoil at a position of 13.3% of the chord measured from the leading edge. The geometry of the NACA0018 profile with the location of the pressure transducers is shown in Fig. 2. This location has been chosen because the pressure fluctuations are expected to be highest there. The part of the airfoil containing the pressure transducers has been sealed air tight, except for the circular tube which sticks out of the wind tunnel.

All signals from the pressure transducers and the sinusoidal signal from the function generator are recorded with a National Instruments data acquisition system (NI SCXI-1000). The unsteady data is post processed using a lock-in method, which allows the extraction of the component of the pressure signal at the excitation frequency and determine its phase. The phase of all the signals is determined with respect to the signal generated by the function generator which is driving the amplifier of the speakers. A Hilbert transform is used to obtain a complex harmonic function from the reference signal.

The function generator is tuned to the first transversal eigenfrequency (f=331 Hz) of the wind tunnel with the wing installed, creating a transversal standing wave. The non-dimensional number which indicates the size of the airfoil

compared to the acoustic wave length is the Helmholtz number $He = 2\pi b/\lambda$, with b the semi chord of the wing and λ the acoustic wave length. If He^2 is small compared to unity the acoustic field around the airfoil is called compact and can be locally approximated as an incompressible potential flow, see Dowling and Ffowcs Williams [11] and Landau and Lifshitz [12]. For the case considered here $He^2 \approx 0.25$, which indicates we are at the upper limit for the wing chord to acoustic wave length ratio. When $He^2 \ll 1$ the airfoil in an acoustically forced flow is expected to be similar to moving the airfoil normal to the main flow in a steady uniform flow. The relation between a moving airfoil in a steady uniform flow and a fixed airfoil in a moving flow will be discussed in Section 5.4. Typically the non-dimensional amplitude of the velocity oscillation at the centre of the wind tunnel can reach an amplitude $v'/U_\infty = O(10^{-1})$. Here v' denotes the amplitude of the velocity fluctuation in y-direction in the centre of the test section, where the prime indicates an acoustic velocity, and U_∞ is the free stream velocity.

The value of the reduced frequency k_b can be varied by adjusting the free stream velocity U_∞. For the current setup reduced frequencies in the range of $2.5 < k_b < 10$ can be obtained. In the experiments the Reynolds number, Re, based on the chord length $2b$, varies from 2×10^5 to 7×10^5.

At given flow velocity, lower values of the reduced frequency k_b can only be reached by reducing the chord length (c) to test section width (L) ratio c/L.

3. Acoustics without main flow

Since the Mach number in the measurement is about $M_\infty = 0.19$ or lower, the convective effect of the flow on the acoustic field is expected to be small. Therefore an analysis of the acoustics without main flow yields a reasonable first order approximation. The measurements are carried out in a wind tunnel where the transversal velocity fluctuations are associated with a transversal acoustic standing wave. Due to the complex geometry of the wind tunnel the acoustic behavior is not trivial. A very simple (and crude) model to describe the acoustical properties of the test section in a wind tunnel is to consider the test section as a square duct of infinite length, see Mosher [8]. However, the test section in the wind tunnel is not infinitely long. The test section has a constant cross section and on the upstream side it is connected air tight to the settling chamber by the contraction. The contraction has an area ratio of settling chamber to test section of about 16 and this area contraction takes place within 1.8 m. This is a rapid area expansion on the length scale of an acoustic wave length $c/f \approx 1$ m, with c the speed of sound and f the frequency in Hz. For plane waves using the Webster approximations, see Dowling and Ffowcs Williams [11], one would expect the configuration to behave like a horn, reflecting waves below 40 Hz, while transmitting higher frequencies. We consider here, however, a transversal acoustic wave which from our numerical simulations appears to reflect. At the other end of the test section on the downstream side there is a slit between the end of the test section and the diffusor, this slit will also reflect acoustic waves. A slightly more sophisticated model than an infinite duct is that of a square duct of finite length, i.e. a duct segment with two open ends.

Initial measurements, on a lose test section without wing, have been carried out in a non rectangular semi-anechoic (the floor is reflecting) chamber with a volume of about 80 m^3. The placement of the test section in the anechoic room enables easy access and provides well defined radiation boundary conditions. These measurements agree within 5% with numerical simulations using a commercial boundary element method SYSNOISE [13]. From the numerical simulations and the measurements we conclude that the acoustic field in a duct segment with two open ends is essentially 2D, due to the influence of the open ends. The resonance frequency is a function of the length of the duct and asymptotically approaches the limit of an infinite duct. For the specific duct segment considered here the resonance frequency was found to be 368 Hz in the experiment and 370 Hz in the numerical model, which agrees well with the formula given by Blevins [14] for an open-open duct.

A measure for the amount of damping in a system is the quality factor, $Q = f_0/\Delta f_{3\,\mathrm{dB}}$. Here f_0 is the resonance frequency and $\Delta f_{3\,\mathrm{dB}}$ is the width of the resonance peak 3 dB below the resonance peak. The quality factor in the numerical model is about 60, while it is 20 in the experiment. This indicates that there are significant energy losses other than radiation losses. Possible explanations for the deviations between experiment and numerical model are wall vibrations, small geometric deviations between the actual setup and the mesh used, and the simplified model to represent the loudspeakers. Visco-thermal losses are not expected to be significant. However, even though the energy losses are not correctly modelled the agreement of the spatial distribution of the predicted pressure field with experiments is good.

With the wing installed the resonance frequency drops to 341 Hz in the experiment and 346 Hz in the numerical model, where the wing was modelled as a flat plate to simplify the analysis. A computation with the exact geometry of the wing yields a resonance frequency of 344 Hz and only small deviation of the acoustic field near the wing are observed, compared to the flat plate model. If the wing chord ($2b$) were comparable to the wind tunnel width (L) a pure Parker-β mode would appear, resulting in a localisation of the acoustic field around the wing, see Parker [15]. Even though the chord of the wing is much smaller than the width of the test section we still observe some localisation.

Fig. 3 shows a contour plot of the acoustic field in the test section with wing installed. The acoustic field has an approximately half cosine spatial dependence in the y-direction and approximately a half sine dependence in the x-direction.

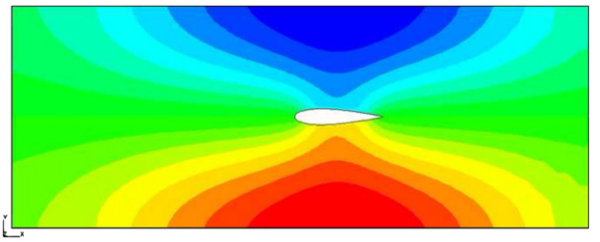

Fig. 3. Qualitative contour plot of the imaginary part of the acoustic pressure in the test section with wing installed.

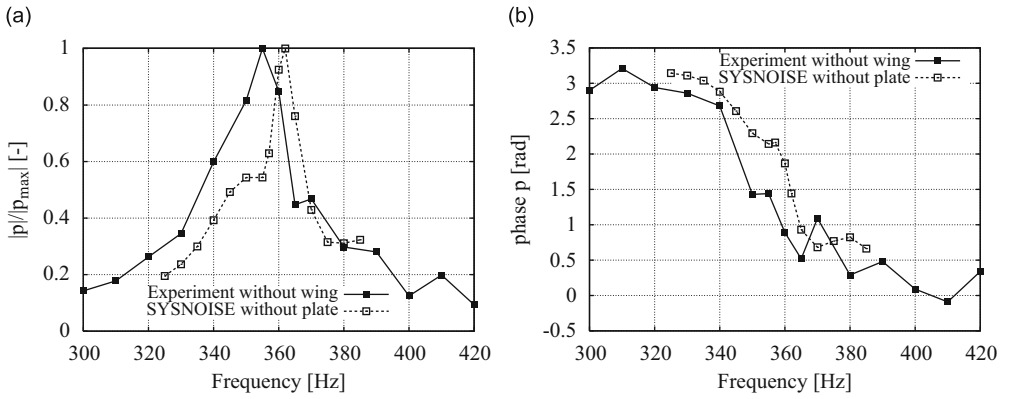

Fig. 4. Amplitude of the pressure and corresponding phase in the test section while placed in the wind tunnel, as a function of the frequency, without wing installed. Measured by microphone M2. Experiments are indicated by the solid line with solid squares. The phase is determined with respect the signal from the function generator. An arbitrary shift in phase is added to the numerical data to allow easy comparison.

3.1. Test section in wind tunnel without wing

The test section is placed back in the wind tunnel. The presence of a contraction and settling chamber upstream of the test section and the slit/diffusor downstream will make the acoustic field complex. The influence of the gap, between the test section and the diffusor, is expected to depend mainly on the width of the gap. In the current case the width of the gap is about 20 mm, which is short compared to the wave length (1 m).

Due to the 3D geometry of the contraction the acoustic field inside the contraction will also be 3D. Therefore a 3D numerical model is needed. In the numerical model the wind tunnel is modelled from the middle of the settling chamber up to 4 m downstream of the slit. At both ends of the numerical model anechoic boundary conditions are imposed. This boundary condition is actually only anechoic for waves at normal incidence. This choice appears to yield a reasonable fit of experimental data. The mesh is refined near the location of the slit. A total number of about 17 500 boundary elements is used for this model.

The acoustic pressure measured by microphone M2 as a function of the frequency, without wing installed, is shown in Fig. 4a, the corresponding phase is plotted in Fig. 4 b. The pressures have been normalised by the maximum value.

In Fig. 4 a it is seen that the resonance frequency is 355 Hz, which is lower than the 368 Hz found for the isolated test section placed in the anechoic room. Measurements of the acoustic pressure distribution in the x-direction, at 355 Hz, are shown in Fig. 5a and 5b, for $y=0.045$ and $z=0.45$ m. The measurements are taken with a microphone which is inserted in the wind tunnel through the slit downstream of the test section. Care is taken to prevent direct contact between the microphone and the wind tunnel walls, this in order to avoid transfer of vibrations. The measured pressure distribution along the x-axis agrees reasonably well with the prediction of the acoustic field by SYSNOISE at 360 Hz. Variation in the z-direction at $x=0.3$ m, were observed in the experimental measurements in the order of 10%, the numerical model predicts very little 3D effects in the test section.

3.2. Test section in wind tunnel with wing installed

Now the wing is installed into the test section and the amplitude and phase are measured at the side wall with microphone M2, the results are shown in Fig. 6a and b. The resonance frequency has shifted to 331 Hz. The numerical model is the same as that used in the previous section, with the exception of the placement of a rigid plate to model the wing, which is modelled by 240 boundary elements. Fig. 7a and b give the results of field measurements of the acoustic field inside the test section placed in the wind tunnel with the wing installed, along the x-direction, with $y=0.045$ and

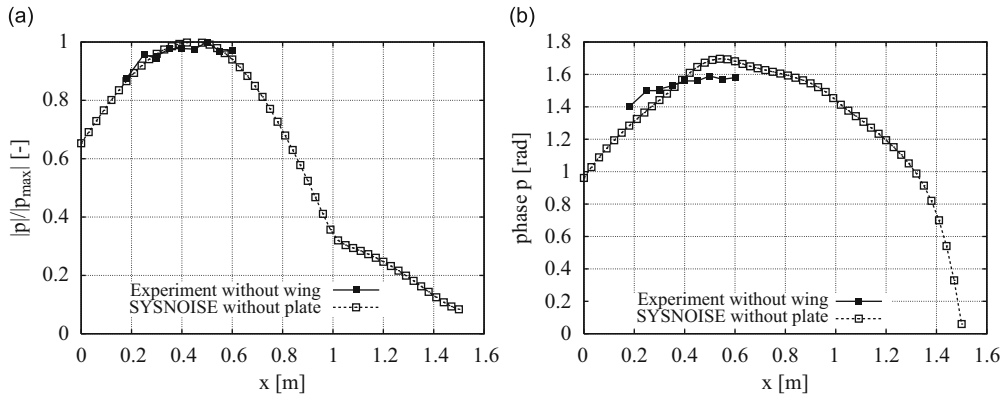

Fig. 5. Amplitude of the pressure and corresponding phase in the test section while placed in the wind tunnel without wing installed, as a function of x. Experiments are indicated by the solid line with solid squares. The phase is determined with respect the signal from the function generator. An arbitrary shift in phase is added to the numerical data to allow easy comparison.

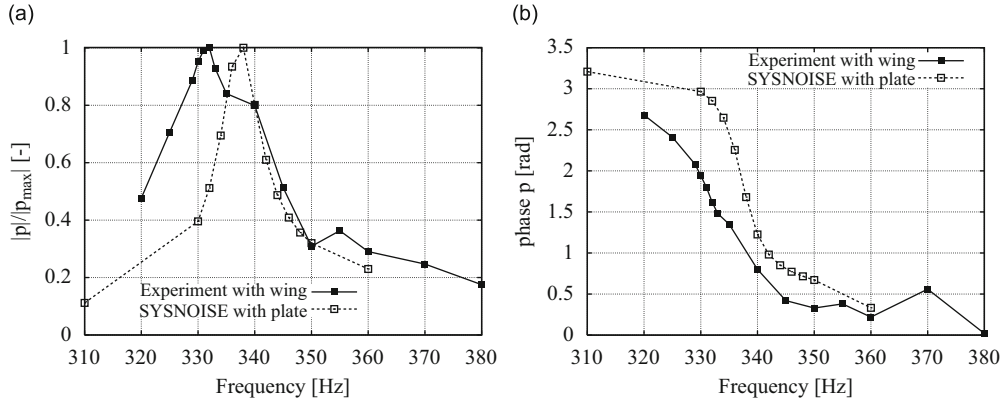

Fig. 6. Amplitude of the pressure and corresponding phase in the test section while placed in the wind tunnel with wing installed, as a function of the frequency. Experiments are indicated by the solid line with solid squares. The phase is determined with respect the signal from the function generator. An arbitrary shift in phase is added to the numerical data to allow easy comparison.

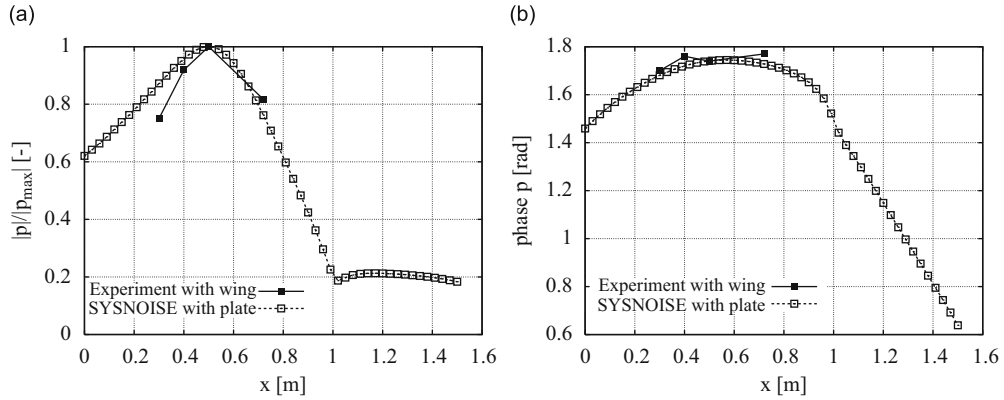

Fig. 7. Amplitude of the pressure and corresponding phase in the test section while placed in the wind tunnel with wing installed, as a function of x. Experiments are indicated by the solid line with solid squares. The phase is determined with respect the signal from the function generator. An arbitrary shift in phase is added to the numerical data to allow easy comparison.

z=0.45 m. We again observe some localisation of the acoustic field around the wing when we compare Fig. 7 a to 5a. In the experimental data a variation in z-direction of about 5% was observed at x=0.3 m. Note that even though the acoustic field inside the contraction and in the diffusor is 3D the acoustic field inside the test section is still almost purely 2D.

3.3. Determination of the transversal velocity

In the previous sections the acoustic field was investigated. We are however interested in the acoustic velocity fluctuations that the airfoil experiences. This means that we need an acoustic model to translate the measured acoustic pressures at the wall into an acoustic velocity in the centre of the wind tunnel at the location of the wing.

Complex notation will be used to define the amplitude of the acoustic pressure measured with the microphones, $p=\hat{p}e^{i\phi}$, with $\hat{p}$ the amplitude and ϕ the phase with respect to the reference signal. The complex $e^{i\omega t}$ convention is used for the complex notation. The acoustic field is assumed to have a half cosine distribution in y-direction, $p'(y)=A\cos\pi y/L$. The amplitude A is determined by the average amplitude of microphones M1 and M2, $A=(p_1-p_2)/2$. From this the acoustic velocity at x=0.3 m is calculated using the linearised Euler equation

$$\rho\frac{\partial v'}{\partial t}=-\frac{\partial p'}{\partial y}. \tag{1}$$

It follows that $v'(y)=(-i\pi A/\rho\omega L)\sin(\pi y/L)$.

4. Numerical model of flow field

So far we have only considered the acoustics without main flow. In order to compute the acoustics in the presence of a main flow, a numerical model based on the Euler equations is used. The numerical method used in this section is a two-dimensional Euler code for internal flows, an Euler code for internal acoustics (EIA) written by Hulshoff [16]. The numerical method is based on a second-order accurate finite-volume spatial discretisation in the interior and a finite-difference discretisation of the compatibility relations on the boundary. The Euler equations are integrated in time using an implicit pseudo-time integration scheme. Numerical dissipation in the code ensures that the Kutta condition is fulfilled at sharp edges. A structured grid is generated with the build-in algebraic grid generator of EIA. A structured grid of 16 blocks is constructed, with an embedded C grid around the profile. Fig. 8 shows a coarse version of this mesh. The total number of cells for this grid is about 4000, with about 64 points per wavelength at the excitation frequency. Since it is impossible to model the three-dimensional contraction and diffusor correctly in two-dimensional space it is chosen not to model the contraction and the diffusor. Furthermore the placement of the wing is expected to localise the acoustic resonant mode. Therefore boundary conditions will be less important in simulations with an airfoil. In the numerical simulations the test section of the wind tunnel is modelled as a duct segment of 2.5 m. The inlet is located 0.838 m upstream of the leading edge of the airfoil. The position of the inlet was chosen such that the acoustic field in x-direction matches the acoustic field in the experiment. At the inlet and outlet of the duct anechoic boundary conditions are applied. Like in the case of the IBEM solution this boundary condition is only anechoic for waves at normal incidence. It appears that these one dimensional anechoic conditions perform reasonably well for the cases considered here. At the downstream side a vortex dissipation zone is added to dissipate vorticity before it leaves the computational domain. This prevents spurious acoustic noise generation. The speakers are modelled as flush mounted moving pistons in the side walls above and below the airfoil.

5. Measurements on a NACA0018 Airfoil

In this section measurements carried out on the NACA0018 airfoil will be presented. First the results in a steady flow will be presented and compared with numerical simulations. Then the results in an unsteady flow with acoustic forcing will be presented and these results will also be compared with numerical simulations.

5.1. Steady flow

As a test case we first consider the case without acoustic forcing, so there is only a main flow in the test section with velocity U_∞. The pressure difference at 13.3% of the chord length from the leading edge is measured for several angles of attack α and is plotted in Fig. 9. The results are presented as a difference in the pressure coefficient, ΔC_p, between the upper and lower side of the airfoil $\Delta C_p=2(p_{\text{lower}}-p_{\text{upper}})/\rho_\infty U_\infty^2$, with ρ_∞ the free stream density. The angle of attack α is defined positive nose-up, as indicated in Fig. 2. Fig. 9 shows that the measurements of the non-dimensional pressure difference at 13.3% chord length from the leading edge agree well with the results of the Euler simulations for small angles of attack. For reference we also give results obtained for an airfoil in free field by means of a potential panel method, for a description see de Jong [17]. The results of the panel code show a slightly higher difference in pressure coefficient, due to the absence of

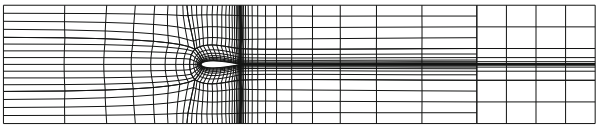

Fig. 8. Figure of a coarse version of the mesh used in the Euler simulations. The vortex dissipation zone is shown at the end of the domain.

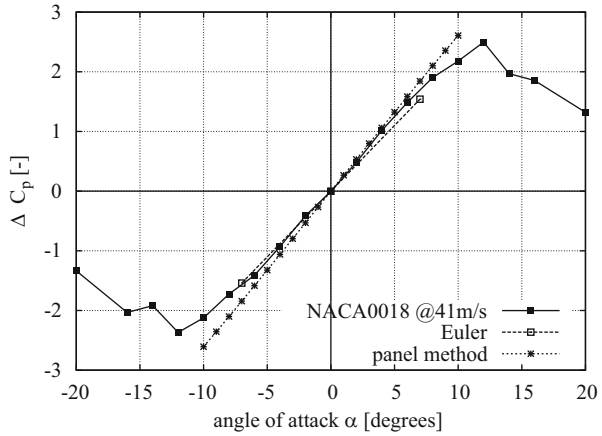

Fig. 9. Non-dimensional pressure difference ΔC_p over the airfoil at 13.3% of the chord from the leading edge as a function of the angle of attack for a standard NACA0018 airfoil (solid line with solid square markers). Also shown are the results of a potential panel method (broken line with asterisks markers) and the results of numerical Euler simulations (broken line with open square markers). The free stream velocity is 41 m/s, Re $=4.5\times10^5$.

wind tunnel walls in this potential panel model. Around $\alpha=10^\circ$ the measurements on the NACA0018 airfoil start to deviate from a straight line, which is an indication that the flow separates from the airfoil.

5.2. Unsteady flow

For the unsteady flow case, the speakers are tuned to the first transversal resonance frequency ($f=331$ Hz) of the wind tunnel with wing installed. The angle of attack of the standard NACA0018 profile is set to zero degrees. The measurements have been performed for several values of the reduced frequency k_b by varying the free stream velocity U_∞. Because the acoustic field has a dependency on x-coordinate also some velocity fluctuations in the x-direction will be generated. The wing, however, is much more sensitive to velocity fluctuations in the normal direction than those in the direction of the flow.

The results are presented in terms of non-dimensional pressure differences, but now the unsteadiness of the flow is also taken into account. This is done by defining an unsteady non-dimensional difference in pressure coefficient

$$\Delta C_{pu}=\frac{\Delta p_u}{\frac{1}{2}\rho_\infty U_\infty v'}, \tag{2}$$

where v' is the acoustic velocity in the centre of the wind tunnel, which is calculated from the measurements of the acoustic pressure at the walls. The subscript u is added to emphasise that this is an unsteady non-dimensional difference in pressure coefficient.

The results are presented in the frequency domain, i.e., as an amplitude and a phase. The phase is determined with respect to the transversal acoustic velocity fluctuation at the centre of the wind tunnel. This transversal velocity is determined at x=0.3 m, from the amplitude of the acoustic pressure measured at the wall of the wind tunnel (see Fig. 1). Note that this location is $1.81b$=149 mm upstream of the airfoil's leading edge. The amplitude of the non-dimensional pressure difference is plotted in Fig. 10a as a function of the reduced frequency k_b and the corresponding phase is shown in Fig. 10 b. Also shown in the figure are results of numerical Euler simulations. In the numerical model the velocity fluctuation is determined in the same way as in the experiments. The agreement between the Euler code and measurements is fair.

5.3. Estimation of plunging velocity

In the previous section data was presented where the acoustic velocity was calculated at x=0.3 m. However, the airfoil experiences a different velocity than that calculated at x=0.3 m. The previous sections have shown that the acoustic field is not one-dimensional and has a dependency on the x-coordinate. The acoustic velocity measured at x=0.3 m by means of microphones M1 and M2 can be corrected for this x-dependency using the measurements of the acoustic pressures in the top wall with microphones M3 and M5. The acoustic velocity previously calculated is multiplied by the ratio of the complex amplitudes of the microphones M5 and M3,

$$v'_{\text{corrected}}=v'_{\text{uncorrected}}\frac{p_5}{p_3}, \tag{3}$$

where $v'_{\text{uncorrected}}$ is the acoustic velocity determined at x=0.3 m. An example of how to calculate $v'_{\text{corrected}}$ is given below.

In order to calculate $v'_{\text{corrected}}$ from pressure measurements at the side walls of the test section, a lock-in method is used to compute the amplitude and phase of the pressure transducers M 1, M 2, M 3 and M 5. The complex pressures will be

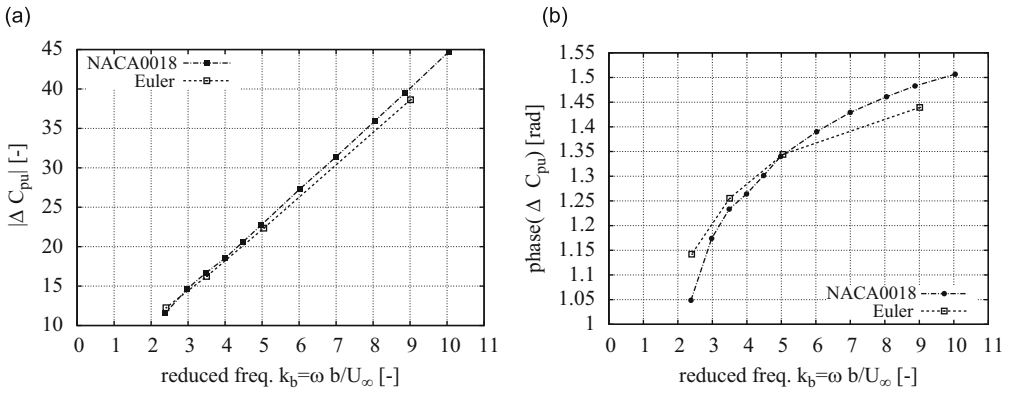

Fig. 10. Amplitude of dynamical non-dimensional pressure difference over NACA0018 airfoil and corresponding phase (solid line with solid square markers), for an amplitude v'/U_∞ varying from 1.4% at $k_b = 2.4$ up to 9.7% at $k_b = 10$. Also shown, the results of Euler simulations (broken line with open square markers), with an amplitude varying from 2.6% at $k_b = 3$ up to 11.4% at $k_b = 9$. The phase is determined with respect to the velocity fluctuation v', at $x = 0.3$ m.

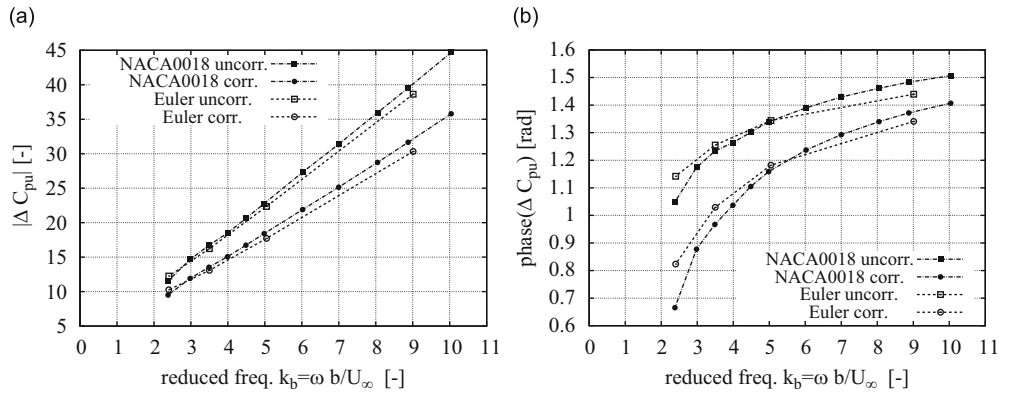

Fig. 11. Amplitude of dynamical non-dimensional pressure difference over NACA0018 airfoil without any correction and corresponding phase (solid line with solid square markers), results of NACA0018 measurements with acoustic correction taken into account (solid line with solid circular markers), for an amplitude v'/U_∞ varying from 1.4% at $k_b = 2.4$ up to 9.7% at $k_b = 10$. Also shown, the results of Euler simulations without correction (broken line with open square markers) and with correction (open circular markers), with an amplitude varying from 0.85% at $k_b = 2.4$ up to 7.5% at $k_b = 9.0$. The phase is determined with respect to the velocity fluctuation v'.

denoted as p'_1 to p'_5. Now we assume a half cosine spatial dependence of the acoustic pressure field in the y-direction, i.e. $p'(y) = A\cos\frac{\pi y}{L}$, and use Eq. (1) to calculate the velocity $v'_{\text{uncorrected}}$ at $x = 0.3$ m. The amplitude A is calculated from the average of the amplitudes of p'_1 and p'_2. The assumption of a half cosine dependence (standing wave) of the acoustic field in the y-direction implies a half sine dependence of the acoustic velocity. Finally the acoustic velocity is corrected by multiplication of $v'_{\text{uncorrected}}$ with the complex ratio of p'_5 and p'_3. As we use the complex ratio the phase is also corrected for.

The results of the measurements are shown in Fig. 11a and b, for the uncorrected data, where the amplitude of the velocity fluctuation is estimated at x=0.3 m and the corrected data, where the x-dependency of the acoustic field is taken into account. Also shown in the figure are results of Euler simulations. The velocity fluctuations in the numerical simulation are calculated from the pressure in the same way as in the measurements and corrected for the x-dependence of the acoustic field by the same procedure as for the experimental data.

The agreement between the Euler code and measurements is fair, considering the application of artificial boundary conditions at the in and outflow, the absence of physical viscosity and the fact that we used a two-dimensional numerical model. The agreement is fair, both for the uncorrected case and for the corrected case. This agreement is an indication that the acoustic field is well resolved by the Euler code.

5.4. Relation to plunging motion

In the previous subsections the experimental and numerical results of the acoustically forced airfoil have been presented. We will now discuss how these results relate to the plunging of the airfoil, where the airfoil is physically displaced with respect to the flow. The fundamental difference between the case of a fixed airfoil in a moving flow and the case of a moving airfoil in a steady uniform flow is the presence of a time dependent uniform pressure gradient in the case

of a moving flow. This pressure gradient is necessary to accelerate the fluid particles of the oscillating main flow. This pressure gradient appears as an extra contribution to the pressure difference over the airfoil analogous to the hydrostatic pressure due to the acceleration of gravity, see Batchelor [18] and Streeter [19].

This contribution to the non-dimensional unsteady pressure difference scales linearly with the reduced frequency and the distance between the two pressure transducers measured in the direction perpendicular to the main flow.

$$\Delta C_{pu} = \frac{2d\cos(\alpha)k_b}{b}, \tag{4}$$

where d is the local thickness of the airfoil. More subtle differences between the acoustic oscillation and the plunging motion are expected due to the effect of the wind tunnel walls. Here we neglect these effects.

For the case of a flat plate without thickness, the problem of a plunging airfoil in a uniform steady flow can be solved by classic linearised potential theory. The local non-dimensional pressure difference is then given by

$$\Delta C_{pu} = 4\left(C(k_b)\tan\frac{\theta}{2} + ik_b\sin\theta\right) \tag{5}$$

here $C(k)$ is known as Theodorsen's function, which is the ratio of modified Bessel functions of the second kind of order zero and order one, and θ is the angle in the transformed plane of the Joukowski transformation used to derive this equation, see Fung [10]. In Figs. 12a and b the results of classical linearised potential theory of Theodorsen are shown by the dotted line and the experimental results for the NACA0018 airfoil are shown by the solid line with solid circular markers. The experiments are corrected for the streamwise dependence of the acoustic field (af) and the contribution of the pressure gradient (pg) due to the moving flow has been subtracted. The correction for the time dependent pressure gradient has been modelled as if the acoustic field were uniform in stream wise direction.

Note that classical linearised potential theory is for incompressible flow with the Helmholtz number equal to zero. As mention earlier, our experiments are performed at a Helmholtz number of 0.5. The effect of the Helmholtz number scales with the Helmholtz number squared. Closed form solutions for the linearised problem in compressible flow can be found in Balakrishnan [20] and Lin and Iliff [21]. These indicate that the effects of non-zero Helmholtz number are of the order of 30%. If one would like to approach the results of classical linearised potential theory the ratio of chord length to test section size should be lowered. A reduction by a factor of two will already reduce the Helmholtz number effect by a factor of four. This effect explains a significant part of the deviations between experiment and theory as observed in Figs. 12a and b. Comparison of experimental data with Euler simulations where a NACA0018 airfoil is plunging in the freefield indicate that other effects such as wall interference and the non-uniform forcing cause a deviation in the order of 10% with respect to a freefield plunging motion.

5.5. Amplitude dependence

One of the advantages of the new measurement technique is that the amplitude can be controlled very accurately within a large dynamical range. The results for difference forcing amplitudes (v'/U_∞) are shown in Figs. 13a and b. The data shown is corrected for the x-dependency of the acoustic field, as described in Section 5.3 and is also corrected for the pressure gradient which is present due to the moving flow. It is seen that there is very little dependence of the amplitude of ΔC_{pu} on the forcing amplitude. There is however an influence of the forcing amplitude on the phase. At higher forcing amplitudes the phase shifts upwards, the shape of the phase remains the same. The amplitude dependence of the phase cannot be understood by potential theory and remains an open question.

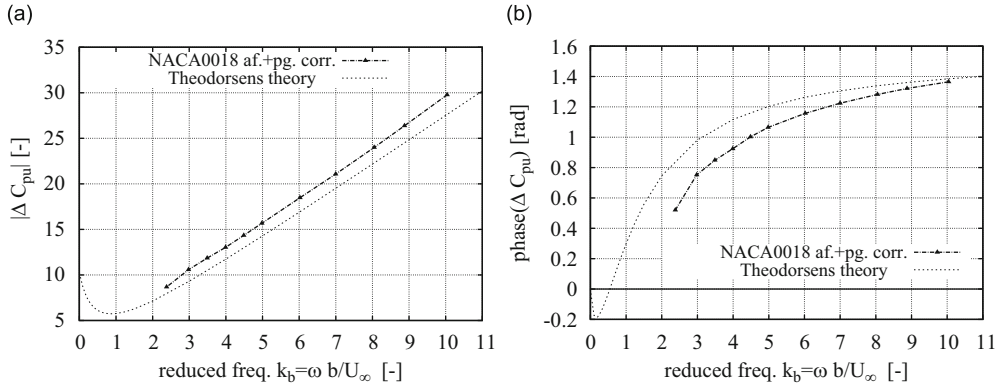

Fig. 12. Amplitude of dynamical non-dimensional pressure difference over NACA0018 airfoil corrected for the streamwise dependence of the acoustic field (af) and corrected for the presence of a time dependent pressure gradient (pg). Also shown by the dotted line the result of classic linearised potential theory for a plunging flat plate. For excitation amplitudes in the range $1.4\times10^{-2} < v'/U_\infty < 9.7\times10^{-2}$. The phase is determined with respect to the velocity fluctuation v', which is corrected for the x-dependency of the acoustic field.

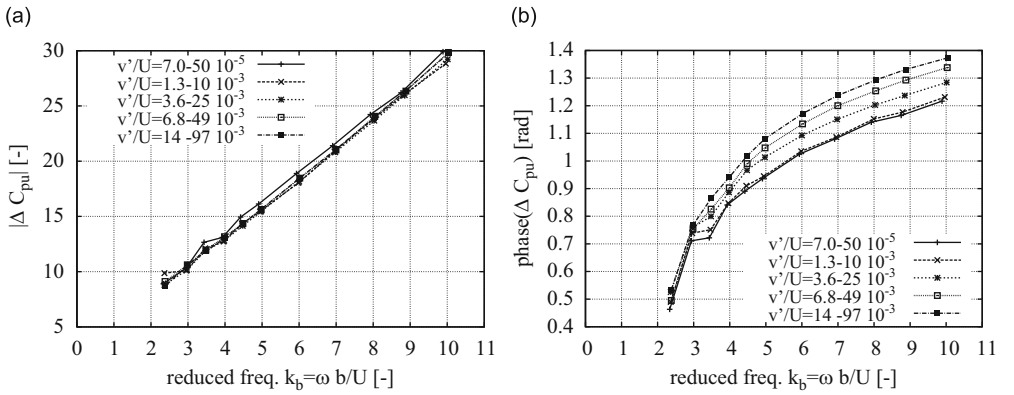

Fig. 13. Amplitude of dynamical non-dimensional pressure difference over NACA0018 airfoil and corresponding phase for different excitation amplitudes v'/U_∞. The phase is determined with respect to the velocity fluctuation v', which is corrected for the x-dependency of the acoustic field.

6. Conclusion

In this paper, acoustic excitation of the first transversal eigenfrequency of the test section inside the wind tunnel was used to simulate the plunging motion of a NACA0018 airfoil. This method can also be applied to other objects besides airfoils, as long as the size of the object is small compared to the acoustic wave length at the resonance frequency. We have only presented local pressure measurements, which restricts the conclusions that can be drawn. However, from Theodorsen's theory it appears that the local pressure difference over an airfoil is closely related to the integrated lift force. Obviously it is possible to use this forcing method in combination with other experimental measurement techniques like PIV, LDA, hotwire or force balance measurement. In our current setup optical access was blocked by the loudspeakers, however these speakers could also be placed in a different configuration to allow optical access. With this new method one can reach high values for the reduced frequency that are difficult to obtain by other means. Furthermore, a strong point of the method is that the excitation amplitude can be varied easily from extremely low amplitudes up to $v'/U = O(10^{-1})$.

Comparison of the experimental data with numerical Euler simulations and linearised potential theory demonstrate that the experimental method works and that the obtained results agree within 10% to a plunging airfoil in freefield conditions. Localisation of the acoustic field due to the placement of the wing makes it difficult to translate exactly the acoustical excitation into a pure plunging motion of the wing, which is a weak point of the proposed method. This problem can be significantly reduced by a reduction of the chord length of the airfoil relative to the test section width. Such a reduction would have the additional advantage of allowing measurements at a lower reduced frequency. If such a reduction is not feasible one can use the procedure proposed in this paper to obtain an estimate for the equivalent plunging velocity amplitude. In spite of this limitation, the method certainly provides an efficient means of exploration of the relative influence of a cavity (or other devices) on the dynamical response of a wing or other object.

Acknowledgements

The authors wish to acknowledge A. Holten, F. van Uittert and G. Oerlemans for technical support. Further we would like to thank C. Schram, I. Lopez and G.J.F. van Heijst for fruitful discussions and suggestions. This work was supported in part by the European Commission within its FP6 Programme under the 'VortexCell2050 project', contract number AST4-CT-2005-012139.

References

[1] VortexCell2050, The VortexCell2050 project funded by the European Commission within its FP6 Programme, contract number AST4CT2005012139 (more information available at www.vortexcell2050.org), 2005.
[2] D. Rockwell, E. Naudasher, Self-sustained oscillations of flow past cavities, *Transactions of the ASME: Journal of Fluids Engineering* 100 (1978) 152–165.
[3] M. Gharib, A. Roshko, The effect of flow oscillations on cavity drag, *Journal of Fluid Mechanics* 177 (1987) 501–530.
[4] R. Halfman, Experimental aerodynamic derivatives of a sinusoidally oscillating airfoil in two-dimensional flow, NACA Report 1108, 1952.
[5] G. Schewe, H. Mai, G. Dietz, Nonlinear effects in transonic flutter with emphasis on manifestation of limit cycle oscillations, *Journal of Fluids and Structures* 18 (2003) 3–22.
[6] K. Zaman, Effect of acoustic excitation on stalled flows over an airfoil, *AIAA Journal* 30 (1992) 1492–1499.
[7] F. Archibald, The laminar boundary layer instability excitation of an acoustic resonance, *Journal of Sound and Vibration* 38 (1975) 387–402.
[8] M. Mosher, The Influence of Wind-tunnel Walls on Discrete Frequency Noise, PhD Thesis, Stanford University, 1986.
[9] I. Lee, Plenum chamber effect on wind-tunnel resonance by the finite element method, *AIAA Journal* 29 (1988) 1087–1093.
[10] Y. Fung, *An Introduction to the Theory of Aeroelasticity*, Dover Publications, New York, USA, 1955.
[11] A. Dowling, J. Ffowcs Williams, *Sound and Sources of Sound*, Cambridge University Press, West Sussex, England, 1983.
[12] L. Landau, E. Lifshitz, *Fluid Mechanics*, 6, Dover Publications, London, England, 1959.

[13] SYSNOISE, by LMS International, Rev. 5.6., 2005.
[14] R. Blevins, *Formulas for Natural Frequency and Mode Shape*, Van Nostrand Reinhold Company, London, England, 1979.
[15] R. Parker, Resonance effect in wake shedding from parallel plates: calculation of resonant frequencies, *Journal of Sound and Vibration* 5 (1967) 330–343.
[16] S. Hulshoff, EIA: an Euler Code for internal acoustics, Part 1: method description and user's Guide, Technical Report, Eindhoven University of Technology, 2000.
[17] H. de Jong, Development of a numerical method for the airflow over a thin layer of liquid, Memorandum M-747 TU Delft, 1996.
[18] G. Batchelor, *An Introduction to Fluid Dynamics*, Cambridge University Press, Cambridge, 1967.
[19] V. Streeter, *Handbook of Fluid Mechanics*, McGraw-Hill Book Company, New York, USA, 1961.
[20] A. Balakrishnan, Unsteady aerodynamics—subsonic compressible inviscid case, CR-1999-206583, 1999.
[21] J. Lin, K.W. Iliff, Aerodynamic lift and moment calculations using a closed-form solution of the Possio equation, TM-2000-209019, 2000.